Chapter 3

Millimetre Very Long Baseline Interferometry

Albert Greve

greve@iram.fr

IRAM, 300 rue de la Piscine, F-38406 Saint Martin d'Hères, France

Millimeter–Wavelength **V**ery **L**ong **B**aseline **I**nterferometry *is interferometry at millimeter wavelengths (3.5 – 1.3 mm: 86 GHz – 230 GHz) with disconnected telescopes using the longest baselines on Earth (1 000 – 10 000 km) in order to achieve the highest angular resolution (0.01 – 0.00005″). The disconnected telescopes need special time/frequency references provided by the observatory–own Hydrogen–masers, synchronized to GPS time signals. The observations are recorded on tape for correlation at special correlator stations. The correlation gives visibility tables. mm–VLBI sees only sources which emit non–thermal radiation at brightness temperatures of $T_B \approx 10^9 - 10^{12}$ K. These sources represent the 'hot' and energetic component of the Universe, for instance masers and quasars.*

3.1 Introduction

Throughout the universe, the common astronomical objects – stars, stellar clusters, molecular clouds, galaxies, AGNs, QSOs, clusters of galaxies – have typical linear dimensions, and only seldom span a factor of 10 to 100 in scale. The more distant the objects, the smaller therefore their apparent angular size, and hence a higher angular resolution and larger collecting area of a telescope is required to distinguish significant structural detail at a significant level of detection. According to a fundamental optics principle, the angular resolution Θ of a full aperture telescope (optical or radio) of diameter $\mathcal{D}$, or of an interferometer consisting of several connected or disconnected telescopes of longest baseline separation $\mathcal{B}$, observing at the wavelength λ, is

$$\Theta \propto \lambda/\mathcal{D} \text{or} \Theta \propto \lambda/\mathcal{B}[\text{rad}] \tag{3.1}$$

If, therefore, the telescope or the baseline has a diameter/length of $\mathcal{D} = \mathcal{B} = \text{n}\,\lambda$, the resolution is

$$\Theta \propto \lambda/\mathcal{D} \;\propto\; \lambda/\mathcal{B} \;\propto 1/\text{n} \tag{3.2}$$

In words, the larger the number (n) of wavelengths spanned by the diameter/baseline the higher is the angular resolution. From these relations it is evident that a high angular resolution is obtained by using short wavelengths (for instance millimeters instead of centimeters), and/or large telescopes, and/or long baselines ([inter]continental distances instead of kilometers). In order to obtain a resolution of $\Theta = 1''$ [the seeing limit at optical wavelengths set by the turbulence of the Earth's atmosphere], the size of the telescope or interferometer baseline must be

$$\mathcal{D}[1''] = \mathcal{B}[1''] \approx 2 \times 10^5, \lambda \tag{3.3}$$

which is $\mathcal{D}[1''] = \mathcal{B}[1''] = 600\,\text{m}$ at $\lambda = 3\,\text{mm}$ (100 GHz). To be comparable in resolution with the HST of $\Theta \approx 10^{-2} \times 1'' = 0.01''$, a telescope/baseline of $\mathcal{D} = \mathcal{B} = 60\,\text{km}$ at $\lambda = 3\,\text{mm}$ is required. To obtain however a resolution of $\Theta = 10^{-2}\times10^{-2}\times1'' = 0.0001'' = 0.1$ *mas* at mm–wavelengths it is evident that the telescope must have Earth dimensions. Such a 'telescope' can only be an interferometer of some sort, of which the telescopes are disconnected and located across a continent, or on different continents, or on different continents and in Space.

The image quality of a mm–VLBI array depends on the available uv–coverage. However, mm–VLBI telescopes cannot be displaced, they are arranged in the given configuration of the observatory sites (see Fig. 3.1), and uv–coverage is only obtained by Earth rotation. The sensitivity of a mm–VLBI array depends on the collecting area and the precision (aperture efficiency) of the participating telescopes.

Very long baseline interferometry, on baseline dimensions of the Earth's diameter and satellite orbits, requires special techniques to record in–phase the different segments of a wavefront emitted by a source and being received by the individual telescopes of the array. This in–phase recording is achieved by locking the oscillators of the receiver and tape recorder unit to a very precise observatory time standard (Hydrogen–maser), which in turn is synchronized to an 'outside clock', available at all stations. This outside clock is provided by time signals of the Global Positioning System (GPS).

3.2 mm–VLBI Arrays

The wet atmosphere, even at high altitudes, has transmission windows at $\sim 3\,\text{mm}$ ($\sim 100\,\text{GHz}$), $\sim 2\,\text{mm}$ ($\sim 150\,\text{GHz}$), $\sim 1.3\,\text{mm}$ ($\sim 230\,\text{GHz}$), and at shorter wavelengths, through which radio signals can propagate to the surface of the Earth. The observing facilities of mm–VLBI, summarized in Table 3.1, make use of these atmospheric windows.

The remark 'Proposal' in Table 3.1 indicates that the array is available to observers on a competitive proposal basis. The 2–mm and 1.3–mm observations are in an experimental state. The mentioned 1.3–mm observations were experimental, and successful.

3.2.1 The CMVA Array

The CMVA (Coordinated Millimeter VLBI–)array contains the telescopes of 12 observatories which operate together in coordinated observations for approximately 15 days per year. The telescopes are located in North–America, Europe, and Chile. The performances of the telescopes at 86 GHz (3.5 mm) are given in Table 3.2, the location of the telescopes is shown in Figure 3.1. The European telescopes of the CMVA are located essentially in the direction North–South, the American telescopes are located essentially in the

Table 3.1: mm–VLBI Arrays and Experimental Observations

Frequency (Wavel.)	Array	Telescopes	Baseline	Observing
86 GHz (3.5 mm)	**CMVA**	Table 2	∼ 8 000 km	Proposal
86 GHz (3.5 mm)	**VLBA**(*)	Table 3	∼ 8 000 km	Proposal
150 GHz (2.0 mm)	—	PV–KP–SEST		experim.
230 GHz (1.3 mm)	–	OVRO–KP	∼ 500 km	experim. (**)
	–	PV–PdBure	∼ 1000 km	experim. (***)

PV: Pico Veleta (Spain), KP: Kitt Peak (USA), OVRO: Owens Valley Obs. (USA), SEST: La Silla (Chile). (*) sub–array of the VLBA array (Table 3.3); (**) [Padin et al. 1990]; (***) [Greve et al. 1995], [Krichbaum et al. 1998]

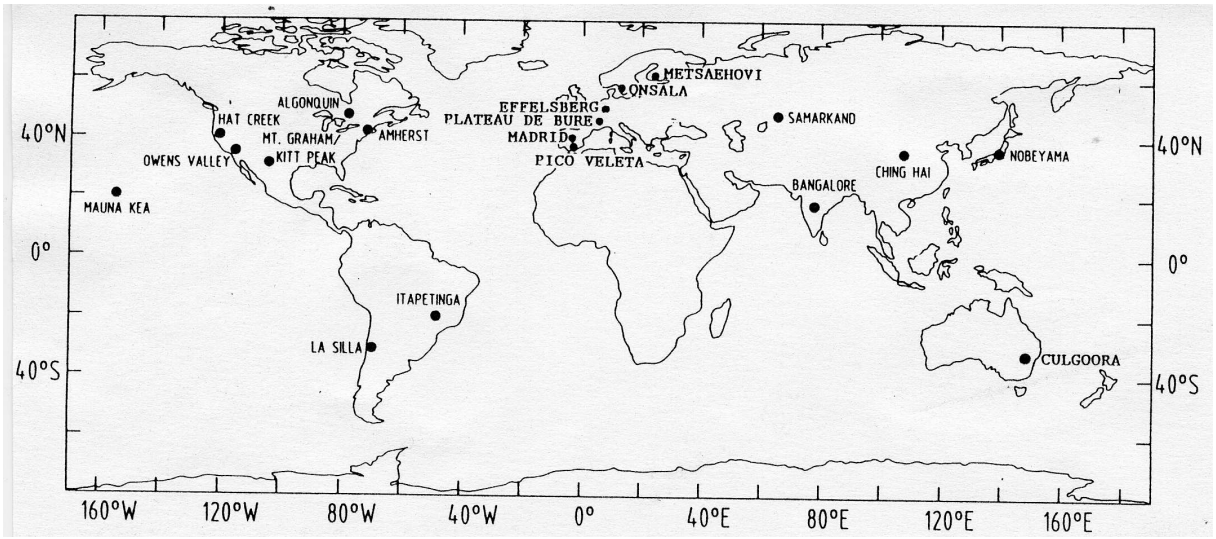

Figure 3.1: Observatories participating in cm and mm–wavelength VLBI. The mm–VLBI observatories of the CMVA (Table 3.2) are concentrated in Western Europe and North America. From [Felli & Spencer 1989], Schilizzi p404, with kind permission from Kluwer Academic Publishers.

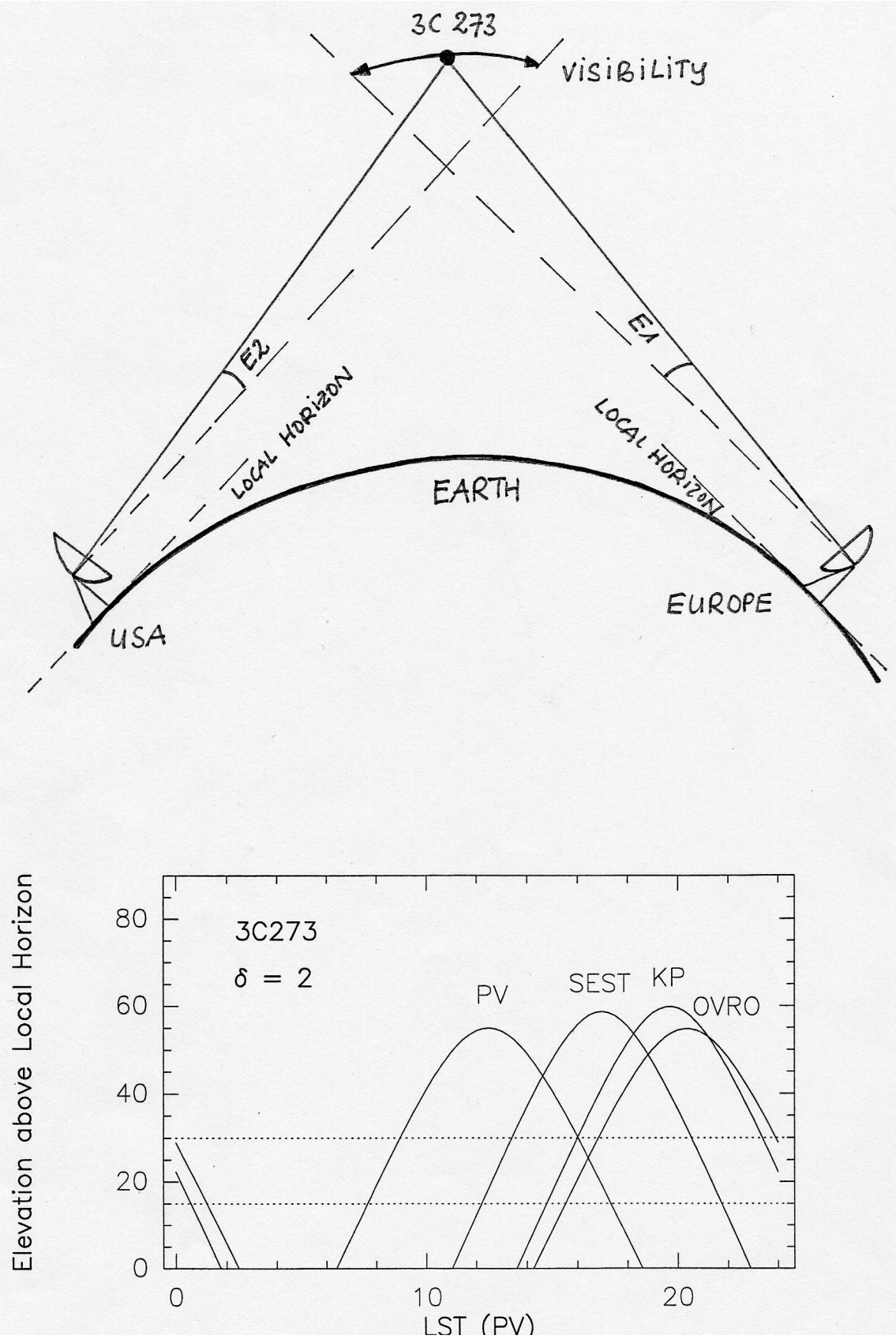

Figure 3.2: Illustration of the low elevation visibility (E_1, E_2) of the QSO 3C 273 (RA: $12^h\,29^m$, Dec: $2^o\,3'$, 1950). The lower part of the figure shows the relative elevation of 3C 273 at Pico Veleta (Spain; LST: local siderial time reference), SEST (Chile), Kitt Peak (USA), and Ownes Valley (USA). The mutual visibility is given by the overlap areas of the individual curves.

Table 3.2: The Coordinated Millimeter VLBI Array = CMVA (86 GHz)

Telescope	Country	$\mathcal{D}$ [m]	T_{sys} [K]	Gain [K/Jy]	η_A	Altitude [m]
CMVA						
Effelsberg	Germany	60	350	0.13	0.13	~ 0
Haystack	USA	37	200	0.058	0.15	~ 0
Pico Veleta	Spain	30	150	0.14	0.60	3000
Onsala	Sweden	20	250	0.056	0.49	~ 0
SEST	Chile	15	300	0.032	0.50	2500
Amherst	USA	14	300	0.024	0.43	~ 0
Metsähovi	Finland	14	300	0.017	0.30	~ 0
(Kitt Peak(*)	USA	12	150	0.023	0.56)	2000
Owens Valley	USA	4×10.4	300	0.067	0.55	1500
Hat Creek	USA	7×6.1	300	0.050	0.65	1000
Expected						
P. de Bure	France	6×15	150	0.045	0.7	2500
GBT	USA	[100]				~ 0
LMT	Mex(–USA)	50				4600
Yebes	Spain	40				500
ALMA	Chile	64×12	(70)	(0.03)	(0.8)	5000

(*) out of operation since July 2000.

direction East–West. As applied in other interferometers, the CMVA array uses Earth rotation to obtain uv–coverage. Some of the strong mm–VLBI sources (3C 273, 3C 279), which are regularly monitored (see Figure 3.9), are located at low declination (Dec = 2^o, -5^o) so that they can be simultaneously observed only at low local elevations, as illustrated in Figure 3.2 for 3C 273 and the stations Pico Veleta – SEST – Kitt Peak – Owens Valley. The low elevation usually implies a high line–of–sight system temperature (T_{sys}), thus a low signal–to–noise ratio, and thus a low detection sensitivity (Sect.3.5). The low elevation implies also that the uv–coverage may be incomplete, the synthesized beam asymmetric, and the final map distorted.

Table 3.2 contains also several telescopes expected to be available in future. These are telescopes with large collecting areas; the dedicated mm–wavelength telescopes (PdB, LMT, ALMA) are located at high altitudes.

3.2.2 The VLBA Array

The VLBA (Very Long Baseline–)array, which consists of 10 dedicated 25–m diameter telescopes (Table 3.3, Figure 3.3), is located on the North–American continent, including one antenna on Hawaii. This array observes routinely at 43 GHz. The array is being upgraded for observations at 86 GHz (3.5 mm); a sub–array (+) is available for 86 GHz VLBI observations. Some of these telescopes collaborate in CMVA observations.

3.3 Available Resolution

Table 3.4 gives an overview of the angular resolution available from the Plateau de Bure interferometer and the CMVA–VLBA mm–wavelength VLBI–arrays (USA + Europe). The table gives for comparison the parameters of the Pico Veleta 30–m telescope (Spain). The table gives also the linear scale corresponding to the angular resolution Θ for a source located at 50 Million pc distance.

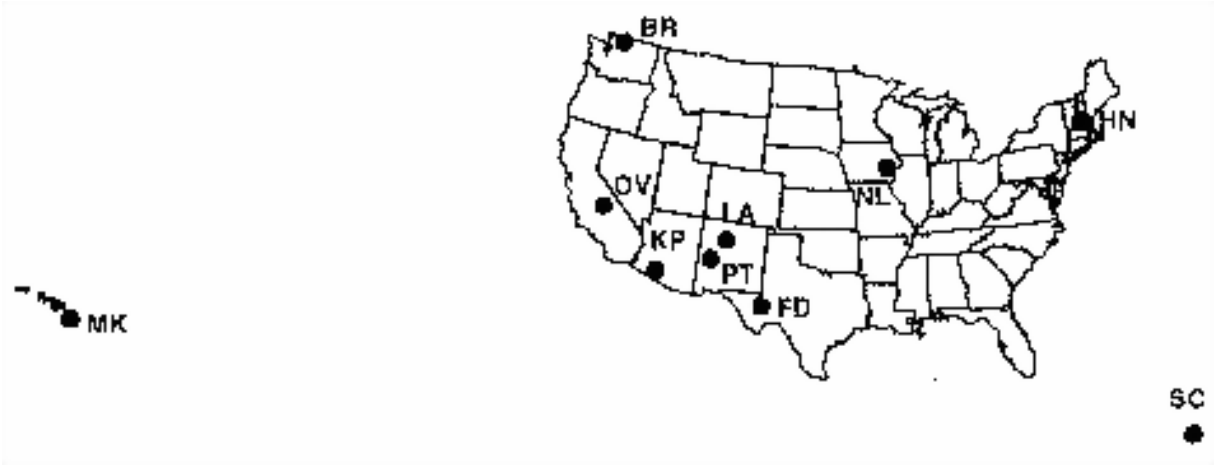

Figure 3.3: The VLBA array (Table 3.3) (from [Zensus et al. 1995]).

Table 3.3: The VLBA Array [10×25 m antennas] (partially operating at 86 GHz)

	Code	Location (USA)	Elevation (m)
	SC	St. Croix VI	16
	HN	Hancock NH	309
+	NL	N. Liberty IA	241
+	FD	Ford Davis TX	1616
+	LA	Los Alamos NM	1967
+	PT	Pie Town NM	2371
+	KP	Kitt Peak AZ	1916
+	OV	Owens Valley CA	1207
	BR	Brewster WA	255
+	MK	Mauna Kea HI	3720

Table 3.4: Diameter ($\mathcal{D}$), Baselines ($\mathcal{B}$), Resolution (Θ), Linear Scale

Diameter/ Baseline	Telescopes	$\lambda = 3.5$ mm $\mathcal{B}/\lambda$	$\lambda = 3.5$ mm Θ	Linear Scale at 50 Mpc
$\mathcal{D} = 0.03$ km	30–m PV (Single Dish)	$8{\times}10^3$	$24''$	6000 pc
$\mathcal{B} = 0.3$ km	PdB (Interferom.)	$8{\times}10^4$	$2.4''$	600 pc
$\mathcal{B} = 1\,500$ km	PV – PdB (VLBI)	$4{\times}10^8$	$0.0005''$	0.1 pc
$\mathcal{B} = 8\,000$ km	CMVA/VLBA (VLBI)	$2{\times}10^9$	$0.000\,09''$	0.02 pc

Table 3.5: Polarization Possibilities (LCP, RCP)

Telescope	Polarization (number of channels, 4 MHz)	Bandwidth
Effelsberg	14 LCP	122 MHz LCP
Onsala	14 LCP	122 MHz LCP
+ Pico Veleta	7 LCP / 7 RCP	56 MHz LCP / 56 MHz RCP
+ Haystack	7 LCP / 7 RCP	56 MHz LCP / 56 MHz RCP
Amherst	14 LCP	122 MHz LCP
+ Pietown	4 LCP / 4 RCP	28 MHz LCP / 28 MHz RCP
+ BIMA	7 LCP / 7 RCP	56 MHz LCP / 56 MHz RCP

3.4 Polarization Observations

The continuum radiation of Quasars (QSO) and the line radiation of SiO masers is polarized, in single dish and interferometer observations from a few percent to $\sim 10\%$ for QSO's, and up to $\sim 70 - 80\,\%$ for the individual components of SiO masers. VLBI observations are normally made at Left Hand–Circular Polarization (LCP = $\mathcal{L}$) in order to eliminate amplitude modulations of a polarized source due to hour angle variations. For polarization observations, measurements are made at LCP and RCP (right hand–circular, $\mathcal{R}$) polarization. The Stokes parameters I,Q,U,V, describing the polarization, and the complex correlations $\mathcal{RR}$, $\mathcal{LL}$, $\mathcal{RL}$, $\mathcal{LR}$ are related by $\mathcal{RR}$ = I + V; $\mathcal{LL}$ = I – V; $\mathcal{RL}$ = Q + iU; and $\mathcal{LR}$ = Q – iU ([Kemball et al. 1995]).

Table 3.5 summarizes the possibility of VLBI polarization observations (status 2000) at 86 GHz. The BIMA (Hat Creek) interferometer can be phased and split into 3 antennas LCP and 3 antennas RCP; this will eventually also be possible with the PdB interferometer.

Polarization observations at 86 GHz of QSO's are so far without convincing success, mainly because of their low degree of polarization; VLBI polarization observations at 86 GHz of SiO masers are in progress.

3.5 The Feasibility of mm–VLBI: Signal–to–Noise Ratio and Detections

The operation and sensitivity, and the present situation and future wishes of mm–VLBI are easily explained from a discussion of the relation expressing the signal–to–noise ratio of an observation with a two–telescope VLBI interferometer. An unresolved source with a size comparable or smaller than the synthesized beamwidth (Θ), measured with both telescopes (1,2), is considered to be detected if the signal–to–noise ratio (SNR) of the observation is ~ 7 or higher, i.e. $7 \leq$ SNR. The relation of the SNR is ([Rogers et al. 1984])

$$SNR = L\sqrt{\eta_1 A_1 \eta_2 A_2/(T_{1,sys}T_{2,sys}) \times 2\tau\Delta\nu} \times (F/2k) \tag{3.4}$$

$$SNR = L(\pi/4)D_1 D_2\sqrt{(\eta_1\eta_2/(T_{1,sys}T_{2,sys}) \times 2\tau\Delta\nu} \times (F/2k) \tag{3.5}$$

with A the geometrical area = π(D/2)^2 and $\mathcal{D}$ the diameter of the telescope (Tables 3.2 & 3.3); η the aperture efficiency (Table 3.2); ηA the effective collecting area; T_{sys} the system temperature (Table 3.2); $\Delta\nu$ the bandwidth (112 MHz for MkIII); τ the integration time; F the correlated flux density; k the Boltzmann constant; and L the correlator efficiency ($\approx 2/\pi$ for a 2–level quantization).

From this relation we note that:

• the incorporation of a large–diameter high–precision telescope significantly improves the performance of a mm–VLBI array. If an array of two telescopes of diameter $\mathcal{D}_1 = \mathcal{D}_2 = 15$ m and efficiency $\eta_1 = \eta_2 = 0.3$ performs at the signal–to–noise ratio SNR(2×15m), the replacement of one telescope by, for instance, the

Table 3.6: SNR for 86 GHz (3.5 mm) Observations: Pico Veleta – Haystack (~ 6000 km)

Source	S(86 GHz) [Jy] (single dish)	SNR (VLBI)
3C 273	25	182–203
3C 279	20	163
3C 345	5.5	6–13
NRAO530	6.5	21–81
1749+096	3.0	21–43
1823+568	2.8	35–43
2145+067	4.5	5–19
3C 454.3	10	78–66

Results obtained at 215 GHz (1.3 mm) on the ~ 1000 km baseline Pico Veleta – PdB are given in Table 3.7 ([Krichbaum et al. 1998]).

IRAM 30–m telescope with $\mathcal{D}_2 = 2\,\mathcal{D}_1 = 30$ m and $\eta_2 = 2\eta_1 = 0.6$ improves the signal–to–noise ratio by SNR(15m & 30m) $= 2 \times$ SNR(2×15m): the array has a 2 times higher sensitivity. It is evident that the future incorporation of the PdB interferometer, the LMT, and ALMA (Table 3.2) will greatly improve the sensitivity of mm–VLBI.

• for observations at mm–wavelengths the location of a telescope at 2000 – 3000 m altitude generally reduces T_{sys} because of the lower amount of atmospheric water vapour, i.e. T_{sys}(high site) $\approx (1/3)\times T_{sys}$(low site) $\approx (1/3)\times(300-500)$ K ≈ 150 K. The lower value of T_{sys} increases the SNR by a factor of 2, or more. Such a decrease of the line–of–sight T_{sys} is especially important for intercontinental/transatlantic baselines where the sources are usually observed at low local elevations (Figure 3.3). Table 3.2 shows that several telescopes of the CMVA array unfortunately are located at low altitudes. Again, the incorporation of PdB Interferometer (2500 m), the LMT (4600 m), and ALMA (5000 m) will greatly improve the sensitivity of mm–VLBI.

• for continuum observations, the foreseen increase in bandwidth of presently $\Delta\nu = 112$ MHz by a factor of two, or more (MkIV), will increase the sensitivity of mm–VLBI by a factor of 1.5, or more.

• the integration time τ is usually limited by the stability of the Hydrogen–maser to values τ(100 GHz) ≈ 1000 s and τ(230 GHz) ≈ 100 s (Sect.3.6). Often however, the integration time is shorter, τ(100 GHz) $\approx$ 100–200 s and τ(230 GHz) $\approx$ 10–20 s, because of phase disturbances introduced by atmospheric water vapour fluctuations. Segmented correlations and atmospheric phase corrections increase the sensitivity of mm–VLBI.

• the SNR is proportional to the *correlated* (unresolved) flux density (F) of the source. At mm–wavelengths it is found that the correlated flux density is often significantly smaller than the total flux density (S) measured with a single dish telescope. It is found, globally, that F $\approx (1/3-1/5)\times$S. As example, for 3C 273 it is observed that S(86 GHz) ≈ 20 Jy while F(86 GHz) ≈ 4 Jy, and S(230 GHz) ≈ 10 Jy while F(230 GHz) ≈ 2 Jy. The presently available CMVA array has sufficient sensitivity to detect sources of total flux density S $\leq 2-3$ Jy.

To illustrate the present situation and possibilities of mm–VLBI, Table 3.6 summarizes the SNR of detections at 86 GHz measured on the baseline Pico Veleta (Spain) – Haystack (USA) ([Krichbaum et al. 1994]; [Beasley et al. 1995]).

3.6 From observations to correlations, step by step

3.6.1 Observing Techniques

A 2–telescope disconnected mm–VLBI array and the (far away) correlator station are shown in Figure 3.4. mm–VLBI observations are made with telescopes separated by several hundreds or thousands of kilometers

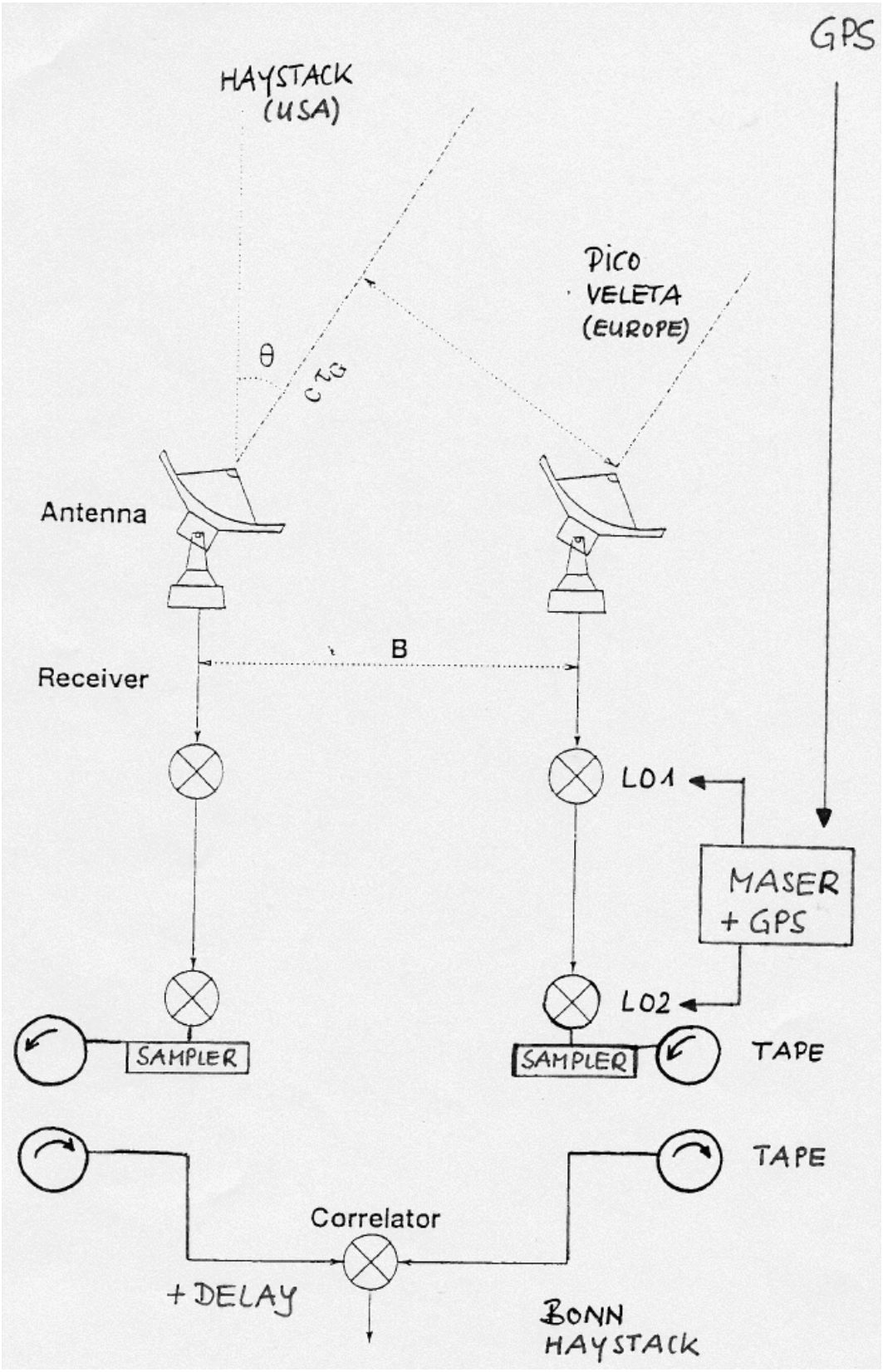

Figure 3.4: Disconnected two–telescope VLBI array; one telescope is located in Europe, the other one is located in the USA. At both observatories, the local oscillators (LO_1, LO_2), the sampler, and the tape unit are locked to the observatory H–maser, synchronized to the satellite GPS time signal. The observations are correlated either at Haystack or Bonn; here the delays and Doppler shifts are introduced.

Table 3.7: SNR for 215 GHz (1.3 mm) Observations: Pico Veleta – Bure ($\sim$ 1000 km)

Source	z	S(215 GHz) [Jy] (single dish)	SNR (VLBI)	F(215 GHz) [Jy] (VLBI)
4C 39.25	0.69	3.5±0.7	< 4	< 0.5
3C 273	0.16	9.2±0.6	7	0.4–0.7
3C 279	0.54	11.0±1.0	35	3–3.8
1334–127	0.54	3.1±0.7	12	0.5–1.1
3C 345	0.59	3.0±0.4	6	≤ 0.4
NRAO530		6.2±0.5	11	0.5–0.8
Sgr A*		4.1±0.5	6	0.5–0.9

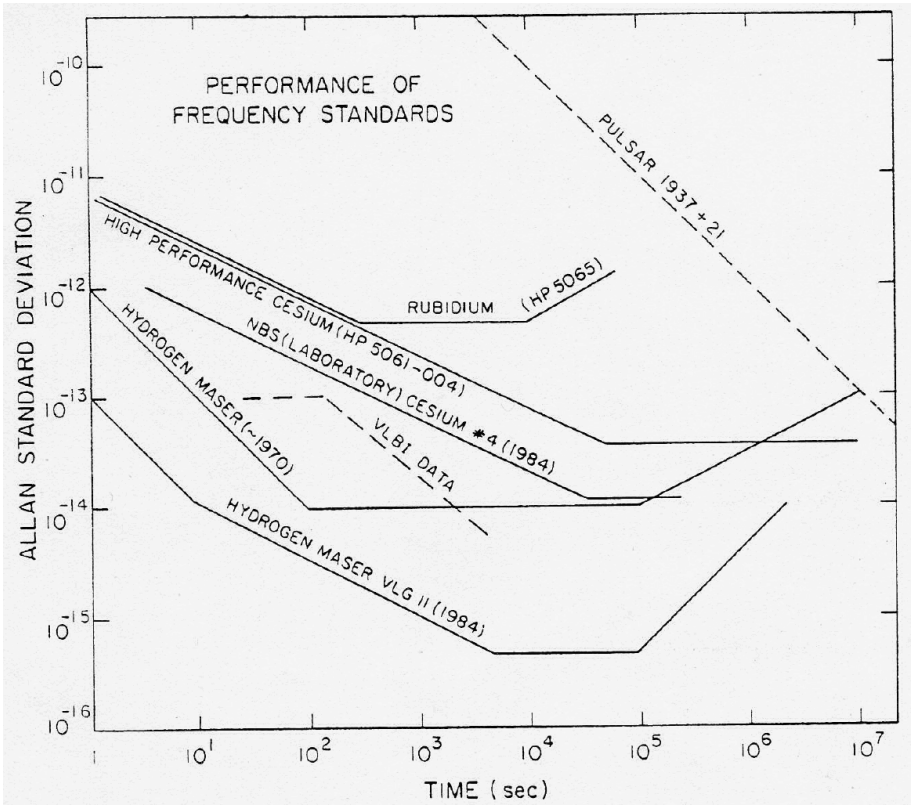

Figure 3.5: Allan standard deviation vs. integrated time for several frequency standards. The phase fluctuations of mm–VLBI are usually dominated by atmospheric phase fluctuations. From [Thompson et al. 1986]. Copyright: @1986 Wiley-Interscience Publications. Reprinted by permission of John Wiley & Sons, Inc.

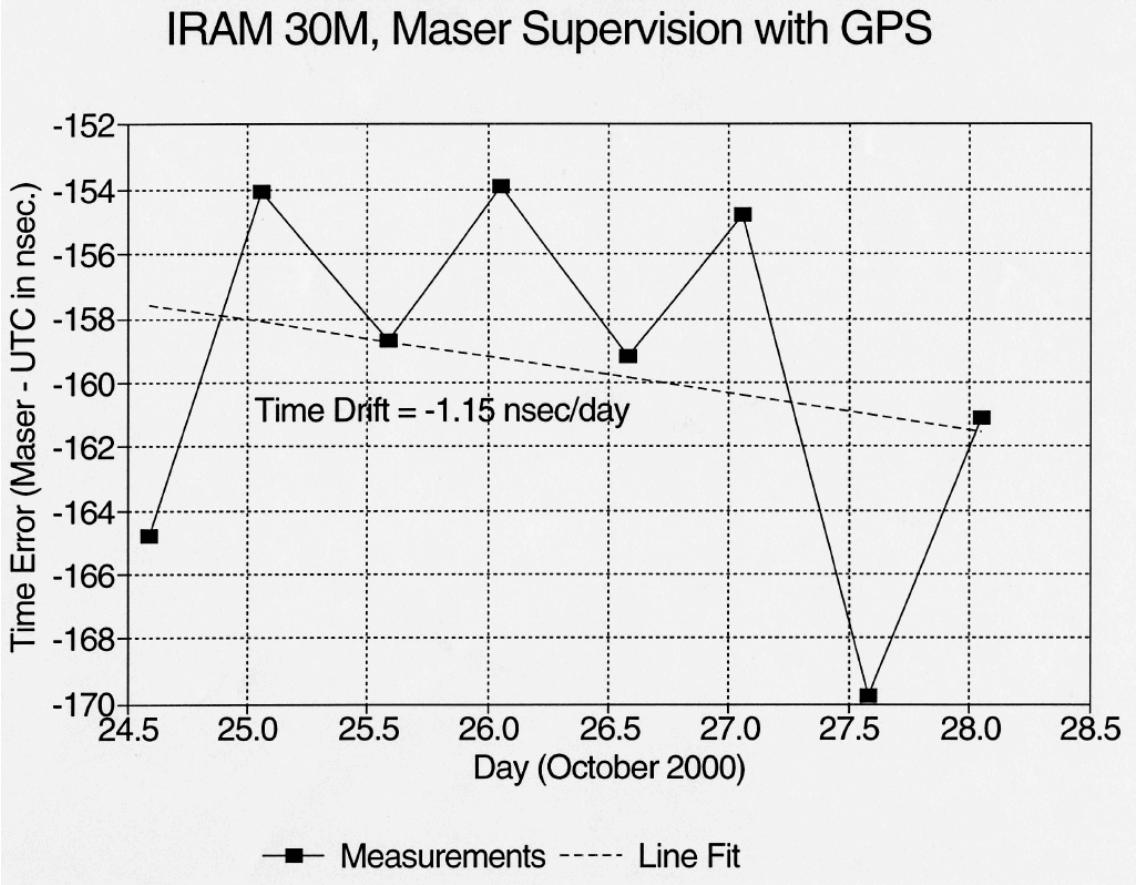

Figure 3.6: Typical H–maser drift measured at Pico Veleta (by courtesy of J. Penalver, IRAM).

not sharing a common time/frequency reference as used in connected interferometry. At each VLBI–telescope therefore the receivers, frequency down–up converters, tape recorders, phase–calibration systems etc. are locked to a Hydrogen–maser which has a typical short–term stability of $\sim 10^{-15}$ and a typical drift of a few 10 nano–seconds per day, or smaller, as shown in Figures 3.5 & 3.6. The VLBI time/frequency systems of the individual telescopes are locked to the GPS system which gives an absolute time reference at the participating telescopes of a few hundred nano–seconds, or better. This time difference must be retrieved a posteriori in the data correlation.

mm–VLBI observations are made at a fixed frequency, preferably at Single–Side–Band tuning in order to reduce noise from the non–used sideband. Fringe rotation and Doppler shifts are introduced a posteriori at the correlator.

3.6.2 Data Recording

In VLBI observations, the telescopes are disconnected and real–time correlation of the signals from the individual telescopes is not possible. At each telescope, the signals are recorded on tape synchronous with the time signal provided by the Hydrogen–maser. In MkIII mode observations, the data are available as 28 channels of 4 MHz bandwidth each; the bandwidth of the recording is $\Delta\nu = 28{\times}4\,\mathrm{MHz} = 112\,\mathrm{MHz}$. The 28 tracks are recorded simultaneously on magnetic tape. The required bitrate of the recording is

$$bits/s = 2 n_c \Delta\nu \tag{3.6}$$

For $\Delta\nu = 112$ MHz and a sampling efficiency $n_c \approx 1-1.6$, the bitrate recorded on tape is ~ 224 Megabites/s. mm–VLBI is being upgraded to 256 MHz bandwidth, and more (MkIV).

3.6.3 Correlation Time

The short–term frequency stability (up to a few 1000 s, see Figure 3.5) of a Hydrogen–maser is $\sim 10^{-15}$. There are long–term drifts which can be checked against GPS signals (see Figure 3.6) and adjusted so that they are below, say, ten nano–seconds per day. The maximum possible integration time (τ) of an observation is set by the requirement that the relative frequency drift $\Delta\nu$ must not exceed, say, $\Delta\nu \approx 0.2$ radians. The integration time then is ([Kellerman & Thompson 1985])

$$\Delta\nu/(2\pi\nu\tau) \approx 0.2/(2\pi\nu\tau) \approx 10^{-15} \tag{3.7}$$

This relation gives $\tau(86\,\mathrm{GHz}) \approx 350\,\mathrm{s} \approx 5$ minutes and $\tau(230\,\mathrm{GHz}) \approx 150\,\mathrm{s} \approx 2$ minutes.

3.6.4 Phase Correction

Because of phase variations introduced by atmospheric water vapour fluctuations, the correlation time τ derived above can be significantly shorter, $\tau \approx 10-30$ s, especially when observing at high frequencies. Because of the scarcity of strong mm–wavelength VLBI sources at sufficiently close distances in the sky, phase referencing as used in connected mm–wavelength interferometry (for instance used on PdB) has not yet generally been applied in mm–VLBI. Efforts are however undertaken to apply phase corrections from local line–of–sight water vapour measurements (sky emission measurements). As an example, the phase stability of a 86 GHz and 215 GHz measurement between Pico Veleta and Plateau de Bure is shown in Fig.3.7. A typical atmosphere–induced phase variation and phase correction applied to 86 GHz VLBI measurements made at Pico Veleta is shown in Figure 3.8.

3.6.5 Correlation

The recorded mm–wavelength VLBI data are correlated at Haystack (USA) or at Bonn (Germany). The end–product of the correlation are calibrated visibility values (uv–tables) which can be used in the same way as data, for instance, obtained with the PdB interferometer.

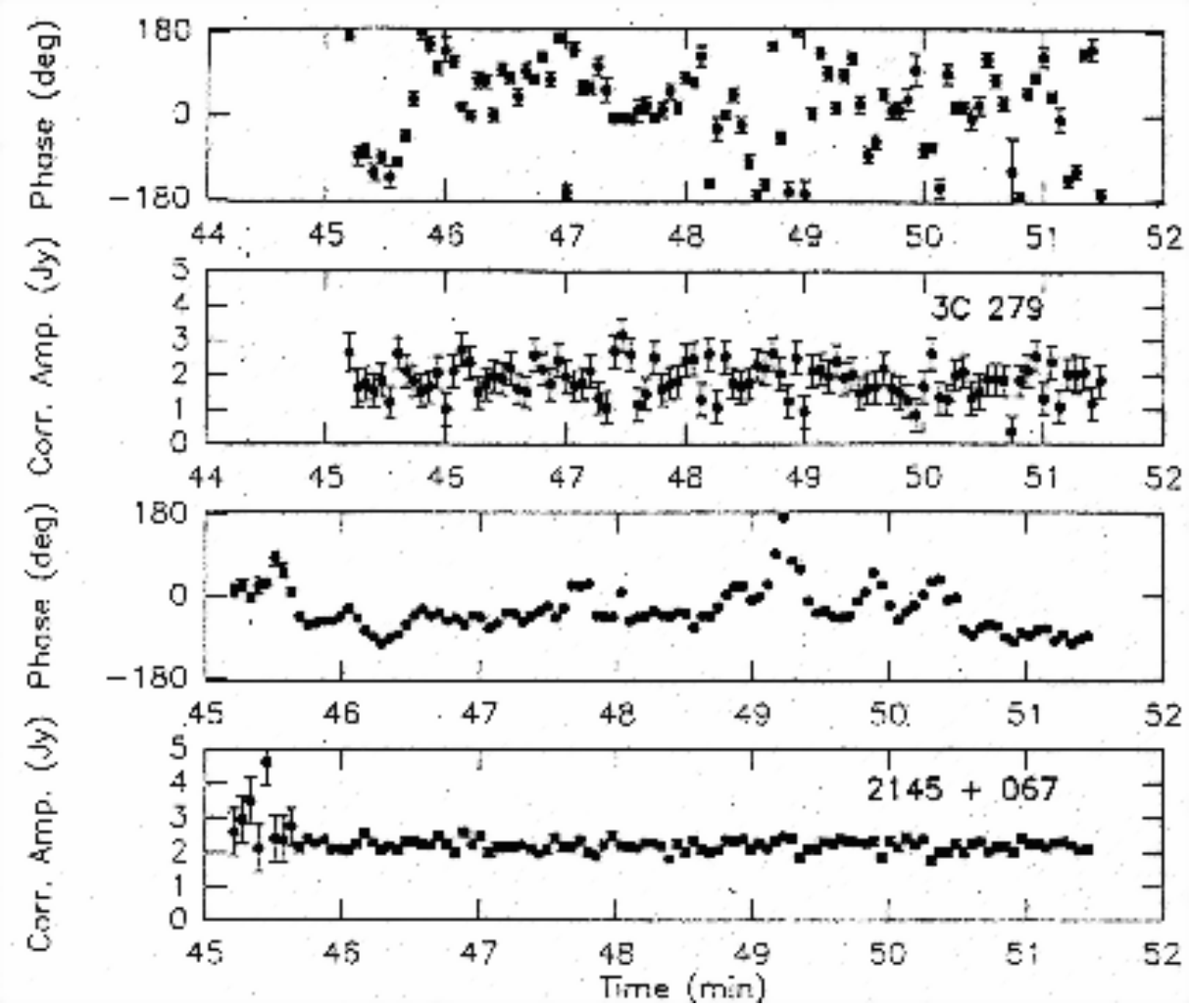

Figure 3.7: VLBI at 215 GHz and 86 GHz between Pico Veleta and Plateau de Bure (1994). The 6.5 minute records show amplitude and phase stability for 3C 279 at 215 GHz (upper panel) and 2145+067 at 86 GHz (lower panel).

3.7 The observable sources with mm–VLBI

3.7.1 Which Kind of sources can we observe

Mm–VLBI sees non–thermal sources emitting, for instance, maser or synchrotron radiation at a high brightness temperature (T_B). The associated astronomical sources are, for instance, masers (SiO) and AGNs and QSOs with jets. mm–VLBI is insensitive to the cold component of the Universe like molecular clouds and other thermal sources. The cold component is observed with interferometers like the Plateau de Bure instrument.

The correlated flux density F of a source with brightness temperature T_B, subtending the solid angle Ω in the sky, is

$$F = (2k/\lambda^2) T_B \Omega \tag{3.8}$$

The correlated flux density ΔF observable within the bandwidth $\Delta\nu$ and integration time τ is

$$\Delta F = (2k/A_{eff}) T_{sys,eff}/\sqrt{2\tau\Delta\nu} \tag{3.9}$$

with $A_{eff} = \sqrt{\eta_1 A_1 \eta_2 A_2}$ the effective surface area of telescope 1 & 2 and $T_{sys,eff} = \sqrt{T_{1,sys} T_{2,sys}}$ the effective system temperature. To arrive at a numerical value of T_B let us assume that we want to detect the source with an accuracy of $\Delta F \approx \epsilon F$, where $0 < \epsilon < 1$. We assume furthermore that the source is unresolved and small and has a size comparable to the VLBI array resolution, hence $\Omega \approx (\lambda/\mathcal{B})^2$. Using these relations we obtain

$$T_B \approx T_{sys,eff} \mathcal{B}^2/(\epsilon A \sqrt{2\tau\Delta\nu}) \tag{3.10}$$

A mm–VLBI array of two telescopes of 15–m diameter, observing at a system temperature $T_{sys,eff}$ = 200 K, a bandwidth of $\Delta\nu$ = 112 MHz, and an integration time limited by the system and atmospheric phase stability to $\tau \approx 100$ s, can only detect sources which have brightness temperatures of $T_B \approx 10^9 - 10^{12}$ K.

3.7.2 The field of view

Evidently, a mm–VLBI array of 8000 – 10 000 km baseline has only a limited field of view (θ_{fov}). Since a disconnected mm–VLBI array does not directly track phase, an estimate of the field of view is obtained by noting that the delay τ between two antennas (see Figure 3.4) separated by the baseline B and observing in the direction θ

$$\tau = (\mathcal{B}/c)\cos\theta \tag{3.11}$$

and that the delay difference $\Delta\tau$ for a small angular displacement $\Delta\theta$ from the main direction of observation is

$$\Delta\tau = -(\mathcal{B}/c)\sin\theta)\Delta\theta \tag{3.12}$$

with c the velocity of light. Since delay corrections are only made in the correlator, the field of view is restricted to directions in which delay smearing ($\Delta\tau$) does not exceed, approximately, $\Delta\tau \leq 1/(2\,\Delta\nu)$. Using this criterion, the field of view is

$$\theta_{fov} \approx \lambda/\mathcal{B}(\nu/\Delta\nu) \tag{3.13}$$

For ν = 86 GHz, $\Delta\nu$ = 112 MHz (MkIII), and $\mathcal{B}$ = 10 000 km we obtain $\theta_{fov} \approx 0.05 - 0.02'' \equiv 50 - 20$ mas.

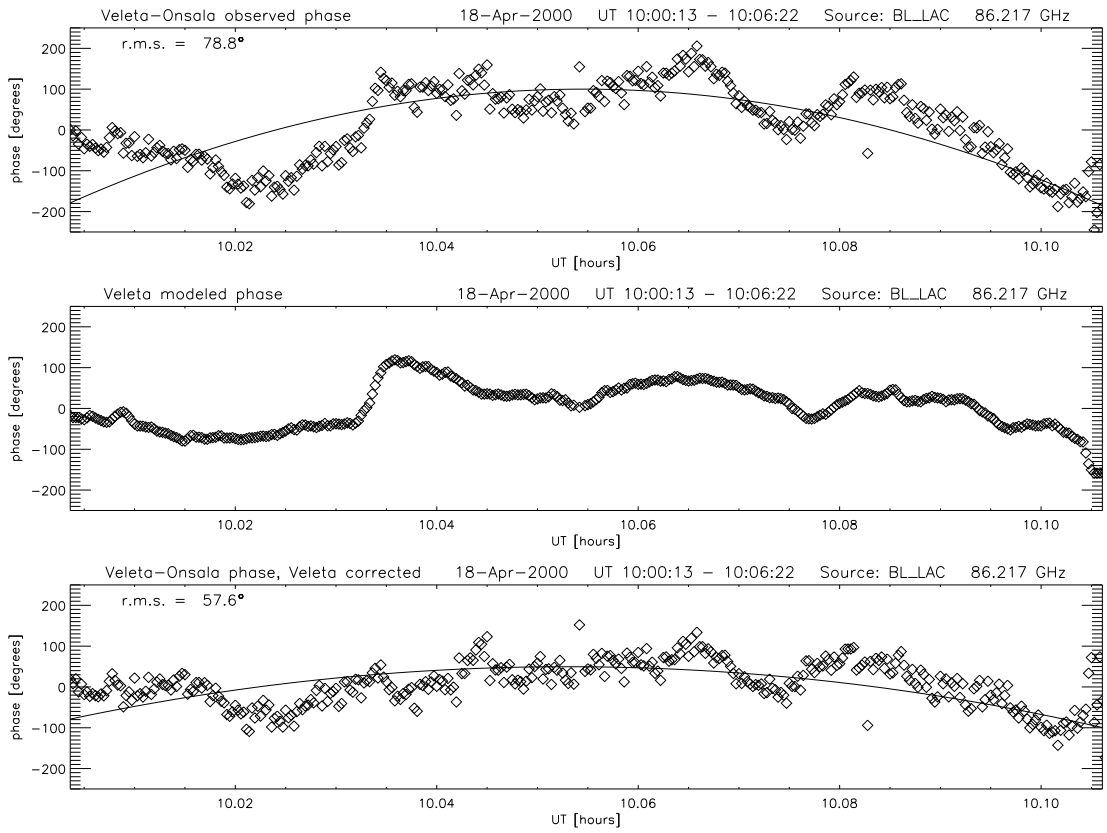

Figure 3.8: mm–VLBI phase correction at 86 GHz. The upper panel shows the phase variation measured on the baseline Pico Veleta – Onsala. The center panel shows the contribution of the phase variation predicted for Pico Veleta from atmopsheric water vapour measurements (200 GHz line–of–sight sky emission). The lower panel shows the improvement in phase stability when the predicted phase fluctuations are taken into account (by courtesy of M. Bremer, IRAM, A. Roy and D. Graham, MPIfR).

3.7.3 An example: mm–VLBI Observations of QSO 3C 273

Fig.3.9 shows observations of the Quasar 3C 273 at 22 GHz (top), 43 GHz (center), and 86 GHz (bottom), performed nearly at the same epochs of 1995.15 (22 and 43 GHz) and 1995.18 (86 GHz). Contour levels in all maps are (–0.5,) 0.5, 1, 2, 5, 10, 15, 30, 50, 70, and 90 % of the peak flux density of 3.0 Jy/beam (top), 5.4 Jy/ (center), and 4.7 Jy/beam (bottom). All maps are restored with the same beam of size of 0.4 x 0.15 mas, oriented at pa = 0^o. The maps are arbitrarily centered on the eastern component (the core); the dashed lines guide the eye and help to identify corresponding jet components in the three maps.

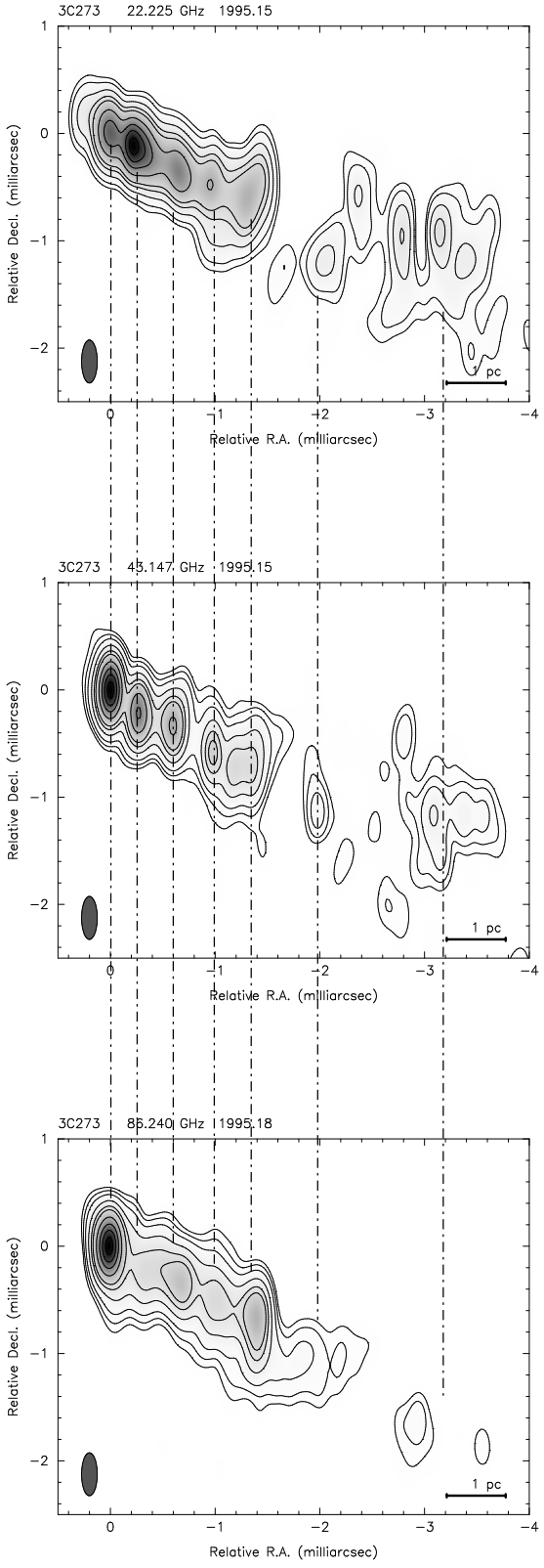

Figure 3.9: VLBI observations of QSO 3C 273 at 22 GHz (1.3 cm) [top], 43 GHz (7.0 mm) [center], and 86 GHz (3.5 mm) [bottom]. The 86 GHz map is obtained from observations with the CMVA array (by courtesy of T. Krichbaum, MPIfR).